Computers and Concrete, *Vol. 15, No. 1 (2015) 73-88*
DOI: http://dx.doi.org/10.12989/cac.2015.15.1.073

Repaired concrete columns with fiber reinforced thixotropic mortar: experimental & FEA approach

Dimitra V. Achillopoulou*, Konstantinia C. Arvanitidou[a]
and Athanasios I. Karabinis[b]

Civil engineering Department, Democritus University of Thrace, Vas. Sofias 12, 67100, Greece

(*Received January 12, 2014, Revised November 3, 2014, Accepted November 9, 2014*)

Abstract. Following previous studies, the current paper describes the results of an experimental program concerning the repair of reinforced concrete columns by thixotropic pseudo plastic mortar, preformed to analyze and quantify the influence of initial construction damage to the behavior of the repaired element. Five columns (section scale 1:2) were designed according to the minimum requirements of reinforcement of ductility orientated codes' design with variables the percentages of initial construction damages. All were tested in axial compression with repeated cycles up to failure. For comparison reasons, another one of the same characteristics, yet healthy, was constructed and tested as a reference specimen. A numerical study (Finite Element Analysis) was conducted for further investigation of the behavior of the thixotropic mortar as repair material. The results indicate that: a) surpassing a specific amount of damage, columns even suitably repaired present lower strain capacity, b) finite element analysis present the same way of deboning of the repaired material taking into consideration the buckling of the reinforcement bars.

Keywords: RC columns; construction damages; repair; fiber reinforced thixotropic mortar, finite element analysis

1. Introduction

Numerous techniques and materials have been applied in retrofit procedure in order to rehabilitate the capacity of crucial reinforced concrete (RC) elements, such as columns. The key of the repair design has proven to be the interface capacity in bearing loads (Vecchio and Bucci 1999; Vitzileou and Palieraki 2007; Austin *et al*. 1999). For this reason the repair material is applied with specific proposed methods indicated by each manufacture according to international standards (EN 206-1. 2000; EN 1504).

Damages in a real structure can be caused by various phenomena through its life time. Briefly, depending on the occasion damages are classified in the following categories:

- Construction imperfections: inadequate consolidation and conservation of concrete before

*Corresponding author, Ph.D., E-mail: dimiachi@civil.duth.gr
[a]Msc Civil Engineer, E-mail: konstantina.arv@gmail.com
[b]Professor, E-mail: karabin@civil.duth.gr

Copyright © 2015 Techno-Press, Ltd.
http://www.techno-press.org/?journal=cac&subpage=8 ISSN: 1598-8198 (Print), 1598-818X (Online)

and after casting, or even due to the existence of large diameter of aggregates in the mixture of concrete which might lead to discontinuity regions (Achillopoulou and Karabinis 2014, Achillopoulou and Karabinis 2013; Achillopoulou *et al*. 2012). Especially in cases where thin-walled sections coexist with other common sections of structural elements, design takes into consideration an average section width. Moreover, design usually disregards regions where the existence of reinforcement is dense and there is no enough space for the aggregate grain to be properly placed. As a consequence, imperfections appear.

- Seismic loads: earthquake loads is the most common reason of structural damages. In cases that the seismic load is greater than the seismic design action, structures present failure in the crucial elements and regions, which varies from cracking of several widths up to disorganisation of concrete (Ludovico *et al*. 2013; Henkhaus *et al*. 2013, Karayannis and Chalioris 2000, Karayannis *et al*. 1998, Karayannis and Sirkelis 2008)
- Exposure to environmental effects: often temperature fluctuation or even ice and froze effects cause significant change to the porosity of the concrete block resulting to barking of the surfaces or even ejection of small parts or total decomposition (Ge *et al*. 2009; Jin *et al*. 2013).
- Corrosion: can be caused by high levels of humidity or long term exposure to water, by carbonation or to chlorides exposure (Kupwade-Patil and Allouche 2013; Sideris and Savva 2005).
- Fire: another common phenomenon. Due to high temperatures (above 600 ℃) concrete loses its capacity in bearing loads. Failure can be instant even in explosive way (Mostafaei *et al*. 2009; Raut and Kodur 2011).
- Time- change of use: in the life time of a structure its use can alter changing in the same time the loads applied. In these cases the sustain reinforced concrete (RC) elements are not capable of standing the extra loads and present fractures or even failure damages. Redesign or even strengthening is usually decided (Fardis 2009).

All above, lead to the impairment of the load capacity of structures. Usually, in real structures a combination of these causes is encountered.

The various codes world-widely (ACI-318R-08 2008; EN1998-3 2005; G.Re.Co.2013) do not quantify the resistance load of elements repaired with each rehabilitation method. What is more, in

Table 1 Requirements according to Standard EN 1504-3

EN 1504-3 Concrete repair product for structural repair CC mortar (based on hydraulic cement)	
Compressive strength	class R4
Chloride ion content	≤0.05%
Adhesive bond	≥2.0MPa
Restrained shrinkage	≥2.0MPa
Carbonation resistance	passes
Thermal compatibility: Part 1: Freeze - Thaw	≥2.0MPa
Elastic modulus	≥25 MPa
Capillary Absorption	≤0.5 $kgr.m^{-2}.h^{-0.5}$
Reaction to fire	A1
Dangerous substances complies with	5.4

Table 2 Repair mortar: mechanical characteristics

Appearance:	grey powder
containing	micro fine fibres
Wet density:	Approx. 2195 kg/m^3
Compressive strength at 25℃ BS 1881: Part 116	>25 N/mm^2 at 1 day >70 N/mm^2 at 28 days
Indirect tensile strength BS 1881: Part 117:	3.6N/mm^2 at 28 days
Resistivity approx.:	12500Ωcm
Water penetration DIN 1048: Part 5:	<5mm

all published studies the overloading effect (Bach *et al*. 2013; Karabinis and Kiousis 2001) is usually examined, though, the factor of extensive imperfections due to inadequate consolidation/ casting deficiencies in combination with loading influence is never analytically referred to. It is decided to quantify and examine the influence of the latter factor to the behavior of columns repaired with thixotropic high strength mortar.

Thixotropic high strength mortars are easy to apply and due to their mechanical properties improve the cohesion between old and new concrete and do not present cracking effect due to slight expansion (BASF Technical Guides 2012; Foti and Vacca 2013). This kind of mortars is produced for application in structural rehabilitation fulfilling the requirements of the R4 category of EN1504-3 standard and the EN1504-6 for steel anchors (Table 1, Table 2). The current study did not include a parametric analysis regarding the mechanical properties of the repair mortar since it is focused more on the application of one kind and the prediction through numerical study of the failure mode of the irregular interface created and on the level of safe prediction through modelling.

The current study adds useful information to previous studies and clarifies the influence of casting deficiencies to the bearing capacity after repair. Also, the numerical modeling (through FEA) of the specimens provides additional information about the behavior of rehabilitation material and its debonding from the interface of the repaired specimen.

2. Experimental investigation

2.1 Specimens' characteristics

In order to examine the influence of the initial construction damage variable in resistance load capacity six specimens were built to simulate reinforced concrete columns in scale 1:2 of rectangular section 150 × 150 m^2 and height 500 mm. The materials used were concrete of approximately 24MPa nominal strength measured cylinder specimens at 28 days, 500MPa nominal yield stress for longitudinal reinforcement and 220MPa for stirrups. Specimens were symmetrically reinforced with two bars of 8mm diameter at each face. Transverse reinforcement

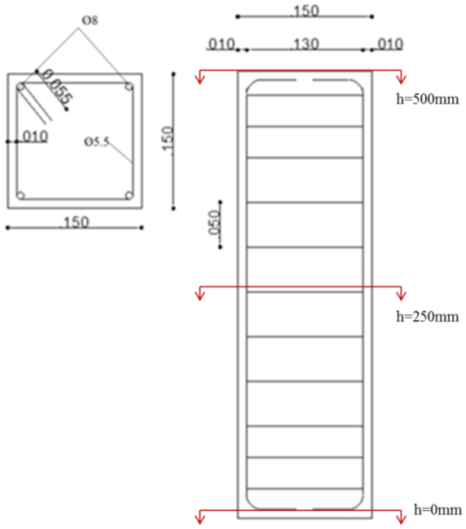

Fig. 1–Cores' reinforcement details

Fig. 2–Construction Damages_D_mR_c-6

(a) Diameter size of vibrator used (b) Aggregate size used

Fig. 3 Incomplete casting

consisted of 5.5 mm diameter spaced at 50 mm (Fig. 1–Cores' reinforcement details Fig. 1). All steel bars were adequately anchored. The concrete specimens represent typical concrete columns sections containing the minimum longitudinal reinforcement ratio (ρ_{min}=0.01) and higher than the minimum ratio of confinement according to medium ductility requirements of modern design regulations at the critical length of structural elements ($\omega_c \geq 0.08$, EN 199-8/3).

During casting consolidation of concrete was incomplete in order to create initial casting imperfections in 9 columns (Fig. 2). Casting was not performed according to the provisions set by EN 206-1 (2000) and ACI 309R-06 (2006) as in real construction sites where it is common to ignore the standards set. According to international standards of concrete consolidation through internal vibration for application of plastic concrete in thin members and confined areas the use of

Fig. 4 Experimental Setup

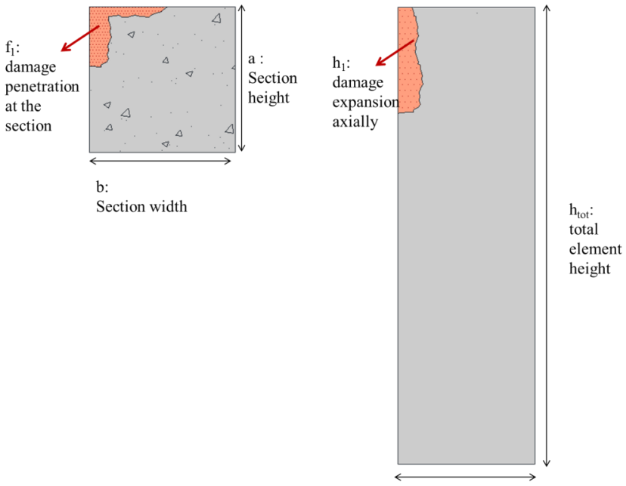

Fig. 5 Schematic damage indexes parameters definition

a 20-40 mm (3/4-1 in) head diameter vibrator is suggested. In this way, the radius of action is 80-150 mm (3-6 in). What is more, the rate of concrete placement is assumed to be within 1-5 yd in the current study, a 20 mm (3/4 in) head diameter vibrator was used and concrete was being placed in higher frequency than predicted (Fig. 3a). What is more, large aggregate size was used (dagr = 32 mm) (Fig. 3b). In this way the casting was considered inappropriate and led to imperfections. One specimen was constructed healthy and considered as reference model. Specimens with casting imperfections were repaired using high strength thixotropic pseudo plastic concrete and were subjected to axial compression repeatedly with cycles of 1‰ axial strain up to 10‰. This pre-loading procedure created overloading cracks as found in real structure member. The axial deformation was measured from the relative displacements between two loading platens with the use of Displacement Transducers (D.T.). The axial load is applied in a compression machine with a capacity of 3000KN maximum load (Fig. 4).

2.2 Quantification of construction damages-deficiencies

In order to quantify the construction damages the model proposed by Achillopoulou&Karabinis (2013) was applied. So as to extract the three indexes, the penetration of damage in the section and its expansion along the height of specimens was measured (Fig. 5). The percentages of those damages to the designed dimensions are extracted through three different indexes:

I) d_s : Section index is the damage ratio of the section d_s = f1 / ftot (Eq. 1)

II) d_h : Axial index which quantifies the expansion axially d_h = h1 / htot (Eq. 2) and,

III) d_v : Volumetric index dv = 1 – [(1-d_s) · (1-d_h)] (Eq. 3)

which combines the above-mentioned indexes resulting to the volumetric ratio of damage.

$$d_s = f_1 / f_{tot} \tag{1}$$

Table 3 Damage indexes of specimens (cores)

Specimen	ω_{wc}	d_s (%)	d_h (%)	d_v (%)
R_c-1	0.15	-	-	-
D_mR_c-1	0.15	25	20	40
D_mR_c-3	0.15	13	24	34
D_mR_c-4	0.15	25	28	46
D_mR_c-5	0.15	37	26	54
D_mR_c-6	0.15	31	22	46

ω_{wc}: mechanical percentage of stirrups

$$d_h = h_1 / h_{tot} \tag{2}$$

$$d_v = 1 - [(1-d_s) \cdot (1-d_h)] \tag{3}$$

Table 3 shows analytically the damage indexes for specimens with minimum levels of ductility of modern codes' design, referring always to ductility orientated design codes.

3. Results

3.1 Experimental results

The influence of the repaired construction damages of specimens is presented by stress- strain curves and energy dissipation diagrams. The maximum stress is obtained at 5 up to 6‰ strain (Fig. 6). The strain values are higher than expected for this kind of concrete. The aggregate size augments the strain values in which maximum response is achieved due to internal sliding between the grains. It is evident that in higher levels of damage - regarding to the levels studied in the current paper- (DmRc-5) the peak stress is more reduced (22%). It should be noted that in cases that the section impairment exceeds 17% (ds>25) (DmRc-5) the failure happens after strain of 5‰ with abrupt load reduction due to early buckling of the longitudinal reinforcement and deboning of repair material(Fig. 7).

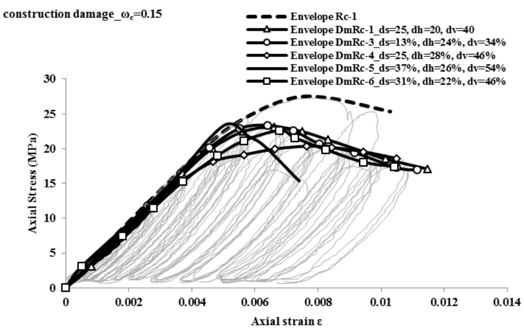

Fig. 6 Construction damage effect on repaired column specimens designed with ductility requirements

Fig. 7 Buckling of longitudinal bar of D_mR_c-5_ω_c=0.15 after failure

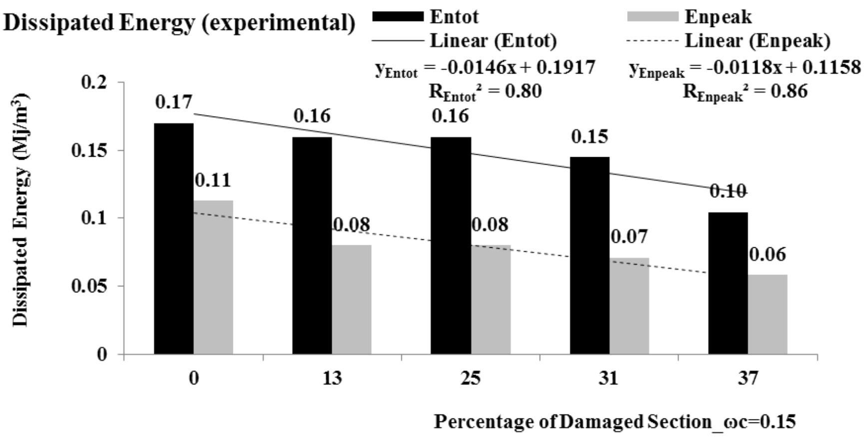

Fig. 8 Dissipated energy of columns with ductility requirements: peak stress-totally

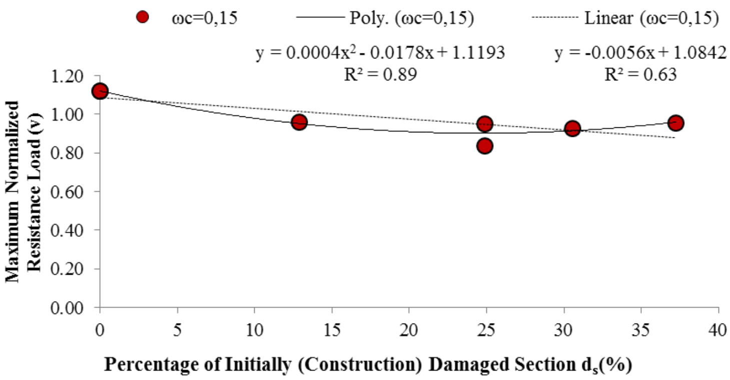

Fig. 9 Association of maximum normalized resistance load (v) with the level of the (construction) damaged section d_s (%)

The dissipation of energy, both up to peak and totally of the repeated loading history of repaired specimens, is lower than the reference specimen. Specimens with damage index up to 25% (DmRc-1, DmRc-3, DmRc-4: d_s=25, 13, 25% respectively) present 27% and 7% reduction in dissipation of energy up to peak load and totally comparing to the reference specimen (Rc-1: d_s=0). In higher levels of damage index the dissipated energy is reduced further up to 45% (DmRc-5: d_s=37%) up to the peak load and up to 40% on the whole, due to the inclination of the abrupt branch presented in the stress- strain curve. All specimen, regardless damages, exceed the 50% of their capacity in dissipating energy up to the peak point of the stress-strain curve (Fig. 8). The tendency of highly damaged specimens (d_s index) to present resistance in lower stress than designed is illustrated graphically (Fig. 9) in order to examine the dispersion. It's sure enough that the error is in tolerable limits since the dispersion factor (R^2) for this level of ductility, is quite satisfactory (0.63), but also the second degree polynomial dispersion factor is in excellent levels (0.89).

3.2 Finite element silmulation and results

A numerical study was conducted using finite element methods in order to examine the accuracy of programs in predicting the failure modes of the repairing mortar and the total capacity of the repaired columns in terms of axial stress and strains, withought the use of complex numerical equations and codes. Moreover, the analysis clarifies the local discontinuities between concrete and repair material. The numerical analysis was performed using a finite element program (Ansys Workbench Tutorials 2013). Isotropic finite element, hexahedral with 20 nodes, was used to simulate concrete, considering bilinear failure criteria by defining the stress strain curve. It should be noted that the analysis lacks the capability of modeling a descending branch in the stress-strain curves for concrete. Interface finite elements, triangular surface with 6 or 8 nodes were used to simulate the interface, considering a delamination and a failure model. The finite elements were chosen according to their ability of simulating homogenious solids with non-linearities and limit the accuracy error, To solve the set of nonlinear- iterative a Newton-Raphson method was used.

The finite element discretization process yields a set of simultaneous equations: $[K]\{u\}=\{F^a\}$ (Eq. 4)

where: $[K]$ = coefficient matrix

$\{u\}$:is the vector of unknown DOF (degree of freedom) values

$\{F^a\}$: is the vector of applied loads

The analysis includes path-dependent nonlinearities, meaning plasticity of concrete. The solution process requires that some intermediate steps are in equilibrium in order to correctly follow the load path. This is accomplished effectively by specifying a step-by-step incremental analysis: the final load vector $\{F^a\}$ is reached by applying the load in increments and performing the Newton-Raphson iterations at each step:

$[K_{n,i}^T]\{\Delta_{ui}\}=\{F_n^a\}-\{F_{n,1}^{nr}\}$ (Eq. 5)

where:

$[K_{n,i}]$:is the tangent matrix for time step n, iteration i

$\{F_n^a\}$:is the total applied force vector at time step n

$\{F_{n,i}^{nr}\}$:is the is the restoring force vector for time step n, iteration i

Taking into account the symmetry of the specimens, only the one quarter was modeled. Even though in the experimental procedure casting deficiencies were not fully symmetric, during repair works the damaged area was cleaned- according to national technical guides (Building Works Standards and Technical Guidelines 2008)- almosta formating a symmetric area. For these reasons and for simplicity of the model, symmetry was chosen by principale. (Fig. 10). The rehabilitation procedure included removal of concrete of the entire damaged region. In this way, a symmetric damage was repaired. The support consisted of restraining all degrees of freedom of the base nodes and the normal displacement. In the symmetry plane all degrees of freedom were also restrained except for the external planes of the specimens, in which the normal displacement was set free. The loading was simulated by external imposed displacement, monotonically, up to 10‰ axial strain (ultimate strain) as performed experimentally. The value of ultimate strain was chosen so as to achieve the peak load and plastic branch in the stress- strain curve. The best mesh was selected in order for the nodes of the different finite elements to coincide. A triangular face mesher was selected for the interface (Fig. 11).

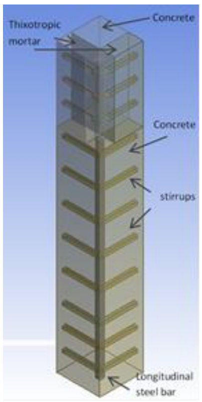

Fig. 10 Symmetrical simulation of damaged column specimen

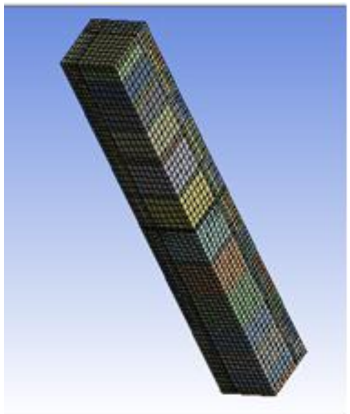

Fig. 11 Discretization of simulated specimen

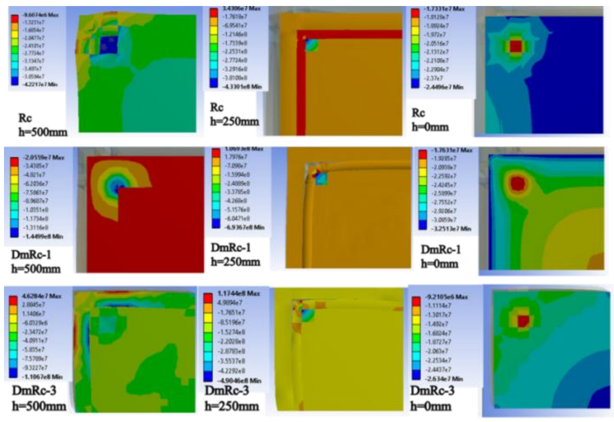

Fig. 12 Normal stress contours of upper (h=500mm), middle (h=250mm) and lower (h=0) section of simulated specimens Rc, DmRc-1, DmRc-3

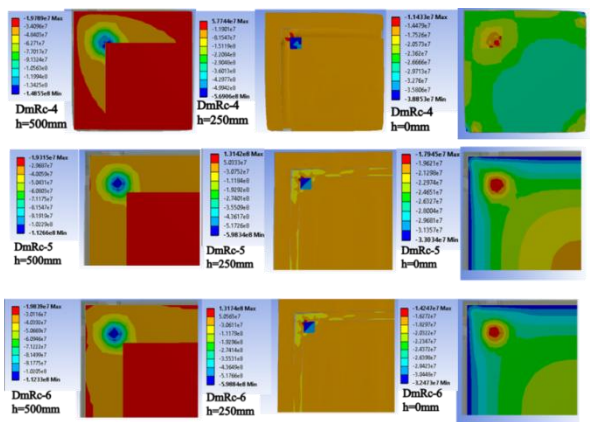

Fig. 13 Normal stress contours of upper (h=500mm), middle (h=250mm) and lower (h=0) section of simulated specimens DmRc-4, DmRc-5, DmRc-6

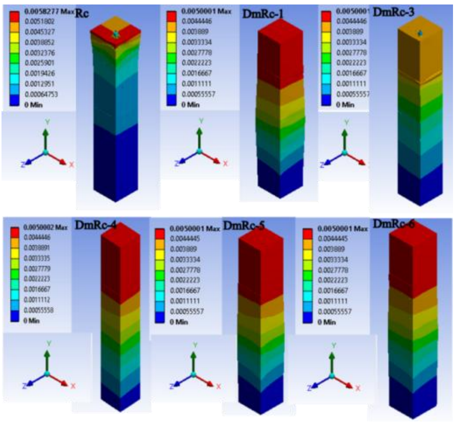

Fig. 14 Axial deformation contour of simulated columns: Rc, DmRc-1, DmRc-3, DmRc-4, DmRc-5, DmRc-6

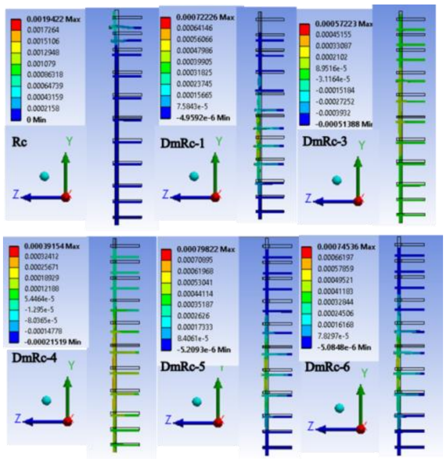

Fig. 15 Buckling of longitudinal reinforcement bars contour of simulated columns: Rc, DmRc-1, DmRc-3, DmRc-4, DmRc-5, DmRc-6

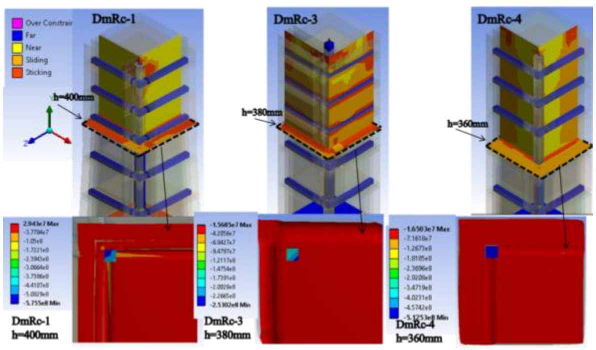

Fig. 16 First section after damage area normal stress contour and interface state for specimens DmRc-1, DmRc-3, DmRc-

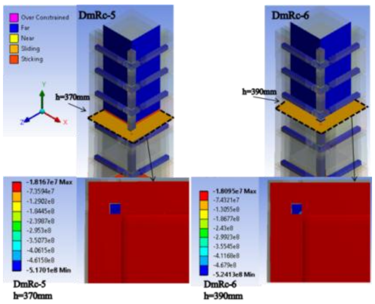

Fig. 17 - First section after damage area normal stress contour and interface state for specimens DmRc-1, DmRc-3, DmRc-4, DmRc-5, DmRc-6

The analysis results are shown in Table 4. The upper section (h = 500mm) presents the higher stress at the confined upper corner. Stresses are gathered around the reinforcement baar due to the expansion of conrete. At specimen Rc the concentration of stress near the confined longitudinal bar is 38% higher than the stress presented at the geometrical center (Fig. 12), proving that the confinement mechanisms are activated and stresses are concentrated at the higher strength obstacle (longitudinal reinforcement bar). Respectively, at specimens DmRc-1, DmRc-3, DmRc-4 stresses are 65%, 74%, 41% higher. At specimens DmRc-5 and DmRc-6, stresses are spectacularly higher around the longitudinal bar (237% and 235% higher respectively) (Fig. 13), stating that when damage exceeds 25% of the section's area, analysis considers that the active section is the residual one.

Gradually, load is expanded at the lower part of the simulated column. As shown in Figures 12 and 13, stirrups are strained the most. All section present small deviation of stress, meaning that after the damaged region, load is fully distributed to the whole section. All damaged specimens present a larger expansion at the middle section. The deformation contour of the whole element is indicatively depicted in Fig. 14. Figs. 15, 16 depict the longitudinal reinforcement bar's buckling. All specimens present the maximum deflection of longitudinal bar at the middle section (h=250mm). All damaged specimens present higher levels of buckling than the reference specimen (Rc). The reference column presented steel reinforcement buckling. Specimens with lower percentage of damaged section (DmRc-1: d_s=25, DmRc-3 d_s=13, DmRc-4: d_s=25), presented up to 86% higher lateral reinforcement deformation, while the rest (DmRc-5: d_s=31, DmRc-6:d_s=37) presented up to 93% higher buckling, in all cases around the middle section (h=250mm). This differentiation is due to the smaller stress relief happening in highly damaged sections. Even with suitable repair the monolithic state is not achieved, in this way the behaviour differs comparing with the reference one.

The analysis confirms the way of the debonding of the repair mortar (Fig. 15). As observed experimentally, at all specimens (Figs. 15, 16) the additional repair thixotropic material gradually is debonded at every load step. The interface –contact- state at the end of the analysis is referred as over constrained, far, near, sliding, and sticking. This particular escalation is relevant to the final position of the interface of the different parts of the element simulated. When the initial boundaries of the interface are exceeded then the options of sliding and sticking are appeared. All other options describe the state before. Specimens DmRc-1, DmRc-3 and DmRc-4 present expansion of core concrete at the damaged area causing normal stress at the interface of the repair material. In this way, interface state can reach up to sticking state, meaning excess of initial interface position. Specimens with higher damaged area (DmRc-5, DmRc-6), present lower expansion of concrete and in this way the original contact state is not affected (Fig. 16). The stress contours of the first section after the damaged area are also presented showing the gradual diffusion of load. The highest level of stress on this section is presented at specimen DmRc-1 with low level of damage impairment and expansion, confirming that the section acts and transfers higher loads than in highly damaged specimens (Fig. 17).

4. Results' discussion

The repaired construction damages seem to affect similarly modeled specimens (Fig. 18). The curves follow the ratio of section impairment which leads proportionally to lower loads. The numerical models result in higher levels of strength and initial chord stiffness. The inclination of the curve up to peak stress is defined as initial chord stiffens. It is remarkable, that excluding the luck of the descending branch of the simulation, the behavior is similar to the experimental. Table 4 presents the values of both experiments and F.E. analysis. What is more, the error of experimental to analysis results are calculated. As peak stress is defined the stress corresponding to inclination altering of the curves, peak strain the corresponding strain and finally, the ultimate strength as mentioned before, the corresponding stress to 10‰ axial strain. For small ratio of section imperfections (Rc-1 d_s=0, DmRc-1 d_s=13), the initial tangential stiffness is overestimated in the F.E. analysis together with the maximum bearing load. The F.E. analysis due to the tangential matrix, calculated from the element stresses and the loads corresponding to the internal forces can be larger. In the experimental procedure the defects of construction can cause the variables in terms of load. What is more, the real exposure conditions of specimens cannot be simulated. The first branch for 13% section deficiency (d_s=13, DmRc-3) presents 27% higher initial chord stiffness, 4% lower peak strength than the experimental one and 25% higher ultimate strength (Fig. 18, Table 4). Though, strain corresponding to the peak load is remarkably lower (38%). For the same ratio of section deficiency (d_s=25, DmRc-1, DmRc-4), the F.E. analysis results in 14-15% higher initial chord stiffness.

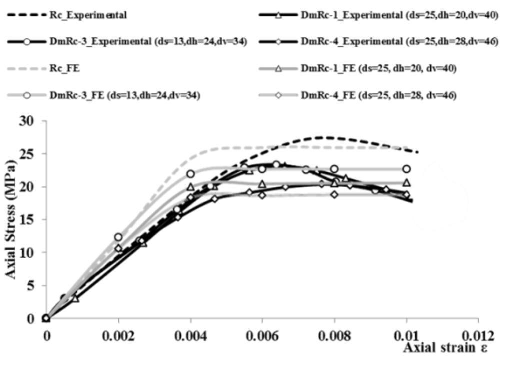

Fig. 18 Comparison of axial stress- strain curves of experimental and analytical results for specimens Rc, DmRc-1, DmRc-3, DmRc-4

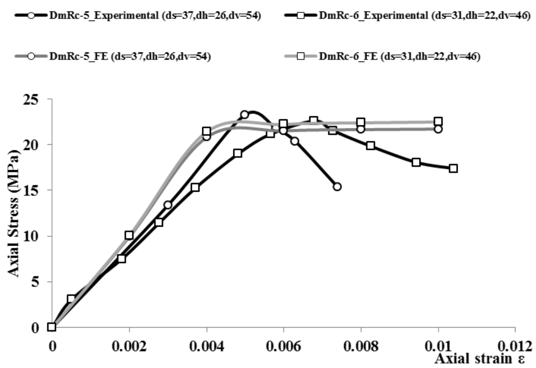

Fig. 19 Comparison of axial stress- strain curves of experimental and analytical results for specimens DmRc-5, DmRc-6

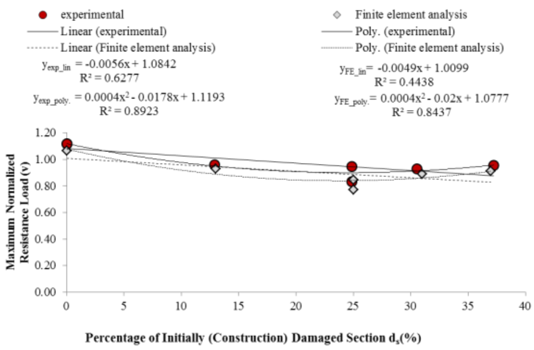

Fig. 20 Comparison of experimental and analytical results association of maximum normalized resistance load (v) with the level of the (construction) damaged section d_s (%)

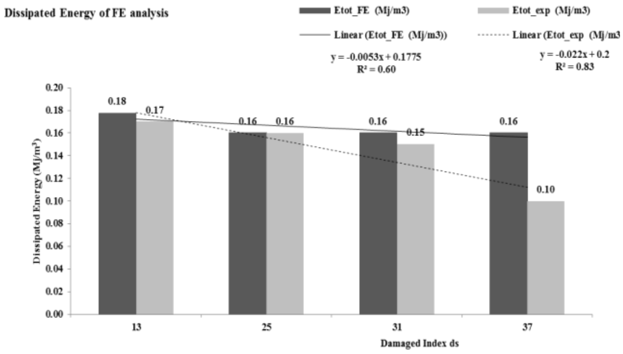

Fig. 21 Total dissipated energy of columns with ductility requirements: comparing experimental research with FEA.

The corresponding strain is also lower (15-40%). For the same damage in the section but lower total damage (d_v) the ultimate strength is 10% higher than the experimental one (DmRc-1). The corresponding strain though is 40% lower.

Specimen with higher volumetric damage (DmRc-4) presented lower augmentation of peak load (1%) but lower reduction of corresponding strain (15%). When the damage index d_s exceeds the limit of 25% (Fig. 19, DmRc-5, DmRc-6: d_s=37-31 respectively), the F.E. analysis is hardly lower in terms of peak stress, up to 6-9% lower than the experimental, but up to 30% higher in the ultimate state. Again, peak strain is up to 75% lower than the experimental, but up to 25% higher in the ultimate state. The difference is remarkable and in terms of dissipated energy both up to peak load and totally. Numerical analysis presents from 11 up to 50% lower dissipated energy up to peak load. Totally, the dissipated energy is up to 33% higher than the experimental procedure. The main differences of all are:

- The capability of redistribution of stress in the F.E. analysis which results in higher stiffness and strain.
- The symmetric simulation of the construction damages which underestimates the damaged region since the possible discontinuities inside the specimen are not modeled.
- The absence of descending branch in the stress-strain bilinear simulation of concrete and the luck of the buckling phenomena of longitudinal steel bars (Fig. 16, Fig. 17). In fact, the buckling effect stops the iteration method and the status of the interface of polymer fiber reinforced, thixotropic repair mortar and other elements appears to be asymmetric (Fig. 18). Though, all other results are totally symmetric.

Both experimental and analytical results prove the tendency of the repaired columns to bear lower loads (Fig. 19). Despite the differences of F.E. and experiments, the association of the maximum normalized load is in the same levels and the dispersion is quite satisfactory (Fig. 20). In all cases load predicted is lower than 1% different than the measured one. Despite this tendency which is pictured in the dissipated comparison diagram (Fig. 21), the totally absorbed energy in medium levels of damaged section (d_s up to 25%), the finite element analysis results are almost coincidental with the experimental results, but on the contrary, in higher damaged section (d_s>30%) there is a reduction of about 40%.

5. Conclusions

Based on the results of the experimental and analytical investigation, the following conclusions are drawn:

1. Initial damages affect the final behavior of the repaired specimen achieving lower values of load.
2. Damage index ds seem to reflect better the reduction of maximum resistance load.
3. The absence of the descending branch in the simulation does not predict the buckling of the longitudinal bars.
4. The ultimate strength together with the total dissipated energy is overestimated again due to the bilinear modeling of concrete curve.
5. Research is necessary in order to improve the prediction of maximum load through the damage indexes.
6. The Finite Element analysis simulation needs improvement through more precise plasticity models.

References

Vecchio, F. and Bucci, F. (1999), "Analysis of repaired reinforced concrete structures", *J. Struct. Eng.*, **125**(6), 644-652

Vintzileou, E. and Palieraki, V. (2007), *Shear Transfer along Interfaces in Repaired/Strengthened RC Elements subjected to Cyclic Actions*, Beton-und Stahlbetonbau 102, Special Edition, 60-65

Austin, S., Robins, P. and Pan, Y. (1999), "Shear bond testing of concrete repairs", *Cement Concrete Res.*, **29**, 1067-1076

EN 1504: European Standard: Products and systems for the protection and repair of concrete structures - Definitions, requirements, quality control and evaluation of conformity, European Committee for Standardization, (April 2013).

Achillopoulou, D.V. and Karabinis, A.I. (2014), "Initial construction damage effect on the behaviour of reinforced concrete columns", *Proceedings of 2nd European Conference on Earthquake Engineering and Seismology*, Istanbul.

Achillopoulou, D.V. and Karabinis, I.A. (2013), "Investigation of shear transfer mechanisms in repaired damaged concrete columns strengthened with RC jackets", *Struct. Eng. Mech.*, **47**(4), 575-598.

Achillopoulou, D.V., Rousakis, T.C. and Karabinis, I.A. (2012), "Force transfer between existing concrete columns with reinforced concrete jackets subjected to pseudoseismic axial loading", *Proceeding of 15th WCEE*, Lisbon.

Di Ludovico, M., Verderame, G., Prota, A., Manfredi, G. and Cosenza, E. (2013), "Experimental behavior of nonconforming RC columns with plain bars under constant axial load and biaxial bending", *J. Struct. Eng.*, **139**(6), 897-914.

Henkhaus, K., Pujol, S. and Ramirez, J. (2013), "Axial failure of reinforced concrete columns damaged by shear reversals", *J. Struct. Eng.*, **139**, SPECIAL ISSUE: NEES 1: Advances in Earthquake Engineering, 1172–1180.

Karayannis, C. and Chalioris, C. (2000), "Capacity of RC joints subjected to early-age cyclic loading", *J. Earthq. Eng.*, **4**(4), 479-509.

Karayannis, C., Chalioris, C. and Sideris, K. (1998), "Effectiveness of RC beam-column connection repair using epoxy resin injections", *J. Earthq. Eng.*, **2**(2), 217-240

Karayannis, C. and Sirkelis, G. (2008), "Strengthening and rehabilitation of RC beam-column joints using carbon-FRP jacketing and epoxy resin injection", *Earthq. Eng. Struct. Dyn.*, **37**(5), 769-790

Ge, Y., Yang, W., Yuan, J. and Zhang, B. (2009), "Effect of inorganic salts on frost resistance of concrete", ICCTP 2009: pp. 1-6

Jin, S., Zhang, J. and Huang, B. (2013), "The relationship between freeze-thaw resistance and pore Structure of concrete", *Pavement and Geotechnical Engineering for Transportation*, pp. 60-67.

Kupwade-Patil, K. and Allouche, E. (2013), "Examination of chloride-induced corrosion in reinforced geopolymer concretes", *J. Mater. Civ. Eng.*, **25**(10), 1465-1476.

Sideris, K.K. and Savva, A.E. (2005), "Durability of mixtures containing calcium nitrite based corrosion inhibitor", *Cement Concrete Compos.*, **27**(2), 277-287.

Mostafaei, H., Vecchio, F. and Bénichou, N. (2009), "Seismic resistance of fire-damaged reinforced concrete columns", *Improving the Seismic Performance of Existing Buildings and Other Structures*, 1396-1407.

Raut, N. and Kodur, V. (2011), "Response of high-strength concrete columns under design fire exposure", *J. Struct. Eng.*, **137**(1), 69-79.

Fardis, M.N. (2009), "Seismic Design, assessment and retrofitting of concrete buildings, based on EN-Eurocode 8'', Geotechnical, geological and earthquake engineering, Springer.

American Concrete Institute (2008), "Building Code Requirements for Structural Concrete (ACI 318-08) and Commentary", ACI -318R-08 Building Code.

European Standard EN (2005), "Eurocode 8 Design of structures for earthquake resistance, Part 3: Assessment and retrofitting of Buildings".

G.Re.Co. Greek Organisation of Seismic Design and Protection (2013), "Greek retrofit code attuned to EN 1998/3" (In Greek).

American Concrete Institute (2008), "Building code requirements for structural concrete (ACI 318-08) and commentary", ACI -318R-08 Building Code.

Bach, A., Stoltz, A., Noldgen, M. and Thona, K. (2013), "Modelling of preloaded reinforced concrete structures at different loading rates", *Proceedings of the 8th International Conference on Facture Mechanics of Concrete Structures*, FraMCoS, 1001-1011, Toledo.

Karabinis, A. and Kiousis, P. (2001), "Plasticity model for reinforced concrete elements subjected to overloads", *J. Struct. Eng.*, **127**(11), 1251-1256.

BASF technical guides for Emaco S88C T Shrinkage compensated, polymer fiber reinforced, thixotropic repair mortar.

Foti, D. and Vacca, S. (2013), 'Mechanical behavior of concrete columns reinforced with rheoplastic mortars", *Mater. Construct.*, **63**(310), 267-282.

European Standard EN (2005), "Eurocode 8 dzesign of structures for earthquake resistance, Part 3: Assessment and retrofitting of Buildings".

EN 206-1: European Standard: Concrete- Part1: Specification, performance, production and conformity (December 2000), European Committee for Standardization.

ACI 309R-06: Guide for Consolidation of Concrete, ACI Committee 309 (May 2006), American Concrete Institute.

Ansys Workbench Tutorials

Building Works Standards and Technical Guidelines (2008), Technical Chamber of Greece

List of symbols

The following symbols are used in the paper:

d_{agr} = aggregate diameter

ω_{wc} = *mechanical ratio of confinement of core*

d_s = ratio of cross-section damage

d_h = ratio of damage axially

d_v = volumetric ratio of damage

f_1 = damage area in cross-section

f_{tot} = cross-section total area

h_1 = length of damage expansion axially

h_{tot} = total height

R^2 = dispersion factor

δ_{peak} = displacement that corresponds to the Peak Load P_{peak}

E_{ntot} = total dissipated energy (MJ/m^3)

E_{peak} = dissipated energy up to peak load (MJ/m^3)

CC